Guide field dependence of 3-D X-line spreading during collisionless magnetic reconnection

L. S. Shepherd[1] and P. A. Cassak[1]

[1] Theoretical arguments and large-scale two-fluid simulations are used to study the spreading of reconnection X-lines localized in the direction of the current as a function of the strength of the out-of-plane (guide) magnetic field. It is found that the mechanism causing the spreading is different for weak and strong guide fields. In the weak guide field limit, spreading is due to the motion of the current carriers, as has been previously established. However, spreading for strong guide fields is bidirectional and is due to the excitation of Alfvén waves along the guide field. In general, we suggest that the X-line spreads bidirectionally with a speed governed by the faster of the two mechanisms for each direction. A prediction on the strength of the guide field at which the spreading mechanism changes is formulated and verified with three-dimensional simulations. Solar, magnetospheric, and laboratory applications are discussed.

1. Introduction

[2] Magnetic reconnection is the basic plasma process in which magnetic energy is converted to kinetic and thermal energies [*Dungey*, 1953; *Vasyliunas*, 1975]. It plays an important role in the dynamics of explosive coronal events, geomagnetic substorms, solar wind coupling to the magnetosphere, and magnetically confined fusion devices. Early models [*Sweet*, 1958; *Parker*, 1957; *Petschek*, 1964] and the predominance of numerical work on magnetic reconnection [e.g., *Birn et al.*, 2001] have treated reconnection as two-dimensional. However, naturally occurring magnetic reconnection often begins in a localized region and spreads in the direction perpendicular to the plane of reconnection. For example, satellite observations of substorms in the magnetotail identified a dawn-dusk asymmetry caused by localized reconnection spreading in the westward direction [*McPherron et al.*, 1973; *Nagai*, 1982]. A similar asymmetry was observed in the formation of arcades in the solar corona [*Isobe et al.*, 2002]. Capturing effects such as these requires a fully three-dimensional treatment.

[3] A number of numerical studies have addressed X-line spreading in the direction of the current during quasi-two-dimensional reconnection. Using a magnetic perturbation localized in the out-of-plane direction in Hall magnetohydrodynamics (Hall-MHD), it was found that the localized reconnection signal propagates as a wave structure carried by the electron current [*Huba and Rudakov*, 2002, 2003]. By seeding reconnection with large random magnetic perturbations in Hall-MHD simulations, it was observed that reconnection develops into spatially isolated structures that lengthen in the direction of the electron current and that these small structures merge into larger-scale structures [*Shay et al.*, 2003]. It was also suggested in this study that spreading occurs in the direction of whichever species carries the current, which need not be exclusively electrons. Spreading by the ions when they carry the current was observed in hybrid simulations with localized resistivity [*Karimabadi et al.*, 2004]. The result of these works is that the reconnection X-line spreads in the out-of-plane direction by the current carriers in the direction of the current carriers [*Lapenta et al.*, 2006]. *Nakamura et al.* [2012] presented the first systematic study to vary the fraction of current carried by each of the species; the results confirmed that X-line spreading occurs due to the current carriers. The results are not dependent on the Harris sheet geometry; *Lukin and Linton* [2011] observed X-line spreading in simulations of island coalescence. Note, each of these studies primarily favored magnetotail applications, so they either treated anti-parallel reconnection or reconnection with a weak out-of-plane (guide) magnetic field compared to the background field. X-line spreading in a system without a guide field was recently observed in laboratory experiments at the Magnetic Reconnection Experiment (MRX), and a physical mechanism for spreading by current carriers was proposed [*Dorfman*, 2012].

[4] Interestingly, experimental and satellite observations of systems with a strong guide field reveal strikingly different behavior of X-line spreading. For example, experiments performed at the versatile toroidal facility (VTF) [*Katz et al.*, 2010; *Egedal et al.*, 2011] exhibit reconnection beginning in

[1]Department of Physics, West Virginia University, Morgantown, West Virginia, USA.

Corresponding author: L. S. Shepherd, Department of Physics, West Virginia University, White Hall, Box 6315, Morgantown, WV 26506, USA. (lshephe1@mix.wvu.edu)

a localized region and spreading bidirectionally in the out-of-plane (toroidal) direction at a speed consistent with the Alfvén speed based on the guide field. Another example is bidirectional spreading (or elongating) of ribbons observed during two-ribbon solar flares [*Qiu*, 2009], including the Bastille Day flare [*Qiu et al.*, 2010]. This presumably is related to spreading of the loop top reconnection site where a sizable guide field is likely to be present. This spreading was also inferred to take place at the local Alfvén speed. Prominence eruptions in the corona have also been observed to spread bidirectionally; this behavior was attributed to magnetic reconnection propagating along the magnetic polarity inversion line (PIL) [*Tripathi et al.*, 2006]. In magnetospheric contexts, observations of extended X-lines several Earth radii long at the magnetopause [*Phan et al.*, 2000; *Fuselier et al.*, 2002] and hundreds of Earth radii in the solar wind [*Phan et al.*, 2006] suggest that X-line spreading occurs in these areas as well, although direct evidence of spreading is prohibitively difficult with single-point or even multipoint satellite observations. X-line spreading was also seen in three-dimensional two-fluid simulations with a guide field [*Schreier et al.*, 2011].

[5] The existing observational data provide a clear indication that the mechanism controlling X-line spreading strongly depends on the strength of the guide field. In the weak guide field limit, the signal is transmitted by the current carriers; in the strong guide field limit, the reconnection signal is transmitted by the magnetic field as an Alfvén wave. We hypothesize that, in general, the X-line spreads in both directions at the speed of whichever mechanism is faster for that direction. In this paper, we present an estimate of the critical guide field where the spreading mechanism changes and confirm the theory with three-dimensional two-fluid numerical simulations.

[6] The layout of this paper is as follows. A prediction of the critical guide field at which the spreading mechanism changes from current carriers to Alfvén waves is developed in section 2. The simulation setup and results are discussed in sections 3 and 4, respectively. A discussion of the results and potential applications is in section 5. We emphasize that we are considering current sheets that are already thin, with large amounts of free magnetic energy present. The important topics of how the sheets become thin and how the magnetic energy is stored are outside the scope of this paper.

2. Theory

[7] Here, we develop a prediction of the speed at which the X-line spreads in each out-of-plane direction as a function of guide field and derive the critical guide field at which the mechanism causing the spreading changes from current carriers to Alfvén waves. To do so, we make the following simplifying assumptions. We treat a quasi-two-dimensional system, meaning that the equilibrium parameters do not depend strongly on the direction normal to the reconnection plane for all time. We assume the current layer is flat, so that the current sheet is either not curved or that the curvature does not strongly contribute to the dynamics. We assume the plasma parameters are symmetric on either side of the current layer; asymmetries [*Cassak and Shay*, 2007] are not considered here. Finally, we assume that a single mode dominates the dynamics; in previous simulations, it was shown that when multiple modes of reconnection occur, they

can impede the spreading of X-lines [*Schreier et al.*, 2011]. This assumption is valid at early times and in systems in which only a single mode is present.

[8] First, we estimate the spreading speed in each direction for each spreading mechanism. We begin with the speed due to the current carriers. From Ampère's law, the current is $\mathbf{J} = c\nabla \times \mathbf{B}/4\pi$, where $\mathbf{B}$ is the magnetic field. For simplicity, we first assume the electrons carry the out-of-plane current, so that the electron velocity is $\mathbf{v}_e = -\mathbf{J}/ne$, where n is the electron density and e is the proton charge. Using a scaling argument, the electron speed v_{eg} in the out-of-plane direction is

$$v_{eg} \sim \frac{cB_{rec}}{4\pi ne\delta}, \tag{1}$$

where B_{rec} is the strength of the reconnecting magnetic field upstream of the electron layer, δ is the thickness of the current layer, and g refers to the direction of the guide field. As has been previously established [*Huba and Rudakov*, 2002; *Shay et al.*, 2003; *Karimabadi et al.*, 2004; *Lapenta et al.*, 2006; *Lukin and Linton*, 2011; *Nakamura et al.*, 2012], this is the X-line spreading speed in the absence of a guide field. In the strong guide field limit, the observations suggest the spreading speed is the Alfvén speed c_{Ag} based on the guide field, given by

$$c_{Ag} = \frac{B_g}{\sqrt{4\pi m_i n}}, \tag{2}$$

where B_g is the strength of the guide field and m_i is the proton mass.

[9] Our hypothesis is that the X-line spreading speed in the direction of the electron out-of-plane flow, which we call v_{Xe}, is the larger of v_{eg} and c_{Ag}:

$$v_{Xe} = \max\{v_{eg}, c_{Ag}\}. \tag{3}$$

From this, one can find the critical guide field $B_{crit,e}$ at which the spreading mechanism changes, where the e subscript denotes the critical field for motion in the direction of the out-of-plane electron flow. Setting equation (1) equal to equation (2) and solving for B_g gives

$$B_{crit,e} \sim B_{rec}\frac{d_i}{\delta}, \tag{4}$$

where $d_i = c/\omega_{pi}$ is the ion inertial length and $\omega_{pi} = (4\pi ne^2/m_i)^{1/2}$ is the ion plasma frequency. Since δ is typically less than d_i as the current is set by electron scales, we expect $B_{crit,e} > B_{rec}$, although $B_{crit,e}$ is on the order of and slightly larger than the reconnecting magnetic field strength upstream of the ion dissipation region.

[10] We perform a similar analysis for the spreading speed in the direction of the ions v_{Xi}. Since electrons carry the current, the ion speed v_{ig} in the out-of-plane direction is

$$v_{ig} = 0. \tag{5}$$

Therefore, the X-line spreading speed in the direction of the ion out-of-plane flow $v_{Xi} = \max\{v_{ig}, c_{Ag}\}$ is given by the Alfvén speed based on the guide field,

$$v_{Xi} = c_{Ag}. \tag{6}$$
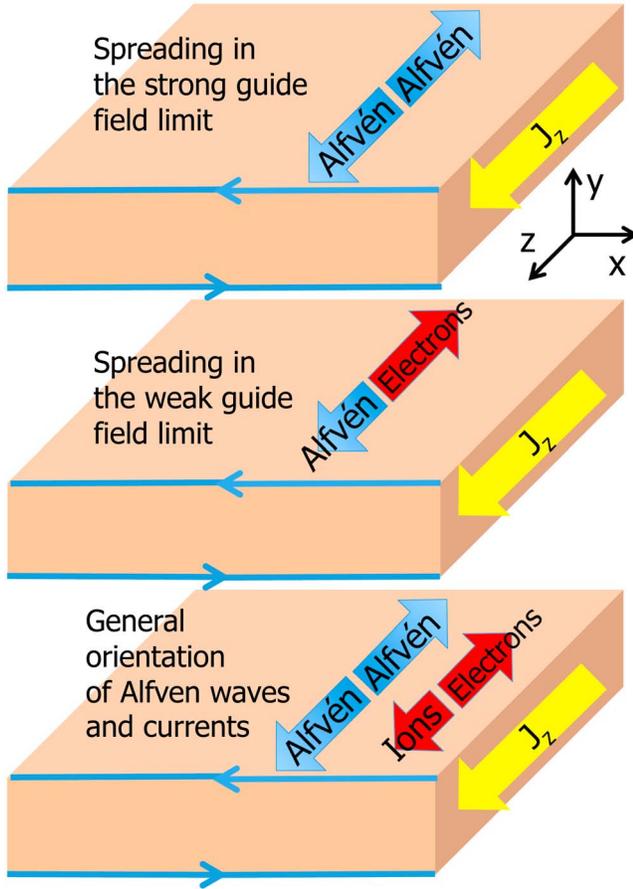
Figure 1. Schematic diagram showing the mechanisms that cause X-line spreading. The thin blue arrows are the reconnecting magnetic field components, and the yellow arrow is the total current. The red arrows denote the speed of the current carriers; the thick blue arrows denote the speed of Alfvén waves along the guide field. The spreading mechanisms for (top) strong, (middle) weak, and (bottom) arbitrary guide field strengths. In each case, X-line spreading occurs at the faster speed in each direction.

Since $v_{ig} = 0$, the critical guide field $B_{crit,i}$ for spreading in the direction of the ion out-of-plane flow is

$$B_{crit,i} = 0. \tag{7}$$

[11] These results can be generalized to systems with both electrons and ions carrying some of the current. Following *Nakamura et al.* [2012], we define the fraction of the total current J_z carried by the ions as α, which is assumed known or measurable. Letting $J_{iz} = \alpha J_z$, one has $J_{ez} = (1 - \alpha)J_z$ so that $J_z = J_{iz} + J_{ez}$. By performing a similar analysis as before, one finds the out-of-plane electron and ion flow speeds due to current carrying are

$$\begin{aligned} v_{eg} &\sim (1 - \alpha)\frac{cB_{rec}}{4\pi ne\delta}, \\ v_{ig} &\sim \alpha\frac{cB_{rec}}{4\pi ne\delta}, \end{aligned} \tag{8}$$

which generalizes equations (1) and (5). The X-line spreading speeds in the direction of the electron and ion out-of-plane flow are

$$\begin{aligned} v_{Xe} &= \max\{v_{eg}, c_{Ag}\}, \\ v_{Xi} &= \max\{v_{ig}, c_{Ag}\}, \end{aligned} \tag{9}$$

respectively, which generalizes equations (3) and (6). Finally, the critical guide fields at which the mechanism for X-line spreading changes from the current carriers to Alfvén waves in the direction of electron and ion flows are given by

$$\begin{aligned} B_{crit,e} &\sim (1 - \alpha)B_{rec}\frac{d_i}{\delta}, \\ B_{crit,i} &\sim \alpha B_{rec}\frac{d_i}{\delta}, \end{aligned} \tag{10}$$

respectively, which generalizes equations (4) and (7).

[12] The predictions derived here are summarized pictorially in Figure 1, where the current is depicted by the yellow arrows and the reconnecting magnetic fields are the thin blue lines. The thick arrows denote the speeds of the current carriers (in red) and the Alfvén speed (in blue) in each out-of-plane direction. The top, middle, and bottom plots show the results for strong, weak, and arbitrary guide field strengths, respectively. In each case, the X-line spreading speed is the longer of the arrows on either side. We point out that there is nothing preventing the spreading mechanisms from being different in the two directions, i.e., Alfvén waves in one direction and current carriers in the other, if that is what equation (9) dictates for the system parameters.

3. Simulation Setup

[13] To test the predictions on X-line spreading, three-dimensional numerical simulations are performed using the two-fluid code F3D [*Shay et al.*, 2004]. The code updates the continuity, momentum, and induction equations with the generalized Ohm's law including electron inertia. Magnetic fields and densities are normalized to arbitrary values B_0 and n_0. Velocities are normalized to the Alfvén speed $c_{A0} = B_0/(4\pi m_i n_0)^{1/2}$. Lengths are normalized to the ion inertial length $d_{i0} = c/\omega_{pi0} = (m_i c^2/4\pi n_0 e^2)^{1/2}$. Times are normalized to the ion cyclotron time $\Omega_{ci0}^{-1} = (eB_0/m_i c)^{-1}$, electric fields to $E_0 = c_{A0}B_0/c$, and temperatures to $T_0 = m_i c_{A0}^2$.

[14] Simulations are performed in a three-dimensional domain of size $L_x \times L_y \times L_z = 51.2 \times 25.6 \times 256.0\ d_{i0}$, where x is the direction of the oppositely directed field, y corresponds to the inflow direction if the simulations were two-dimensional, and z is the direction of the initial current. The plasma is assumed to be isothermal and there is no resistivity ($\eta = 0$). Boundaries in all three directions are periodic, but the system is long enough in the z direction that the periodic boundaries do not affect the dynamics on the timescales of import to the present study.

[15] For simplicity, the simulations have the electrons carrying all of the initial current (i.e., $\alpha = 0$). The electron inertia is $m_e = m_i/25$. In previous simulations with this electron mass (and confirmed in the simulations here), it has been observed that the current layer thickness δ thins down to the electron inertial scale $d_e = 0.2\ d_i$ and the reconnecting magnetic field at the electron layer is $B_{rec} \simeq 0.4\ B_0$ [*Jemella*
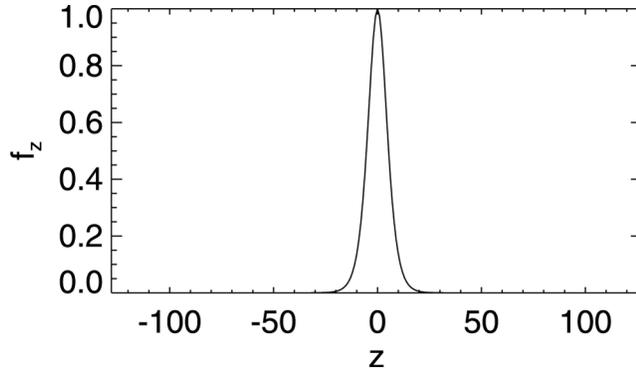
Figure 2. The envelope $f_z(z)$ used to localize the magnetic perturbation in the out-of-plane direction z.

et al., 2003]. Substituting this into equation (4), we predict a critical guide field of

$$B_{crit} \simeq 2 \ B_0. \tag{11}$$

Therefore, we can test the theory by running a series of simulations in which the initial guide fields are $B_g = 0$, 0.5, 1, 1.5, 2, 2.5 and 3. Note, the scaling $\delta \sim d_e$ and $B_{rec} \sim 0.4 \ B_0$ may or may not be representative of naturally occurring reconnection; care should be taken to investigate this for particular applications.

[16] The initial configuration is a double tearing mode with two Harris sheets, $B_{x0}(y) = \tanh[(y + L_y/4)/w_0] - \tanh[(y - L_y/4)/w_0] - 1$, with uniform initial temperature $T = 1$ and a nonuniform plasma density to balance total pressure. Here, $w_0 = 0.4 \ d_{i0}$ is the initial current layer thickness. We choose this thickness to be comparable to the smallest value of the ion Larmor radius $\rho_s = c_s/\Omega_{ci} = \sqrt{T}/B_g \simeq 0.33$, where c_s is the sound speed and the latter expression is written in normalized units. This scale is the Hall scale in the presence of a strong guide field [*Zakharov et al.*, 1993; *Rogers et al.*, 2001]. It is worth noting that the Hall scale increases smoothly from ρ_s to d_i as the guide field is decreased to zero, which follows from a linear analysis of Hall-MHD waves [*Rogers et al.*, 2001]. Consequently, the smaller guide field simulations start with a current sheet that is thin relative to the Hall scale, and should onset rapidly. As the guide field is increased, the time to onset should increase and it is expected that a hyperresistive phase of reconnection will occur before onset. This behavior will not adversely impact our study, as we will separate out the times for which Hall reconnection is dominant.

[17] We employ a grid scale of $\Delta x \times \Delta y \times \Delta z = 0.05 \times 0.05 \times 1.0 \ d_{i0}$. Using a stretched grid in the out-of-plane direction has been done before [*Shay et al.*, 2003], and is acceptable since the in-plane kinetic-scale dynamics is on smaller scales than the out-of-plane dynamics. To ensure the stretched grid scale in the out-of-plane direction does not play a role in the numerics, some simulations are confirmed by comparison with simulations with $\Delta z = 0.5 \ d_{i0}$. All equations employ a fourth-order diffusion with coefficient $D_{4x} = D_{4y} = 2.5 \times 10^{-5}$ in the x and y directions. In the out-of-plane direction the fourth-order diffusion coefficient D_{4g} depends on the speeds in the out-of-plane direction. For $B_g \leq 2.0$ the fourth-order diffusion coefficient is $D_{4g} = 0.064$ and

for $B_g = 2.5$ and 3.0 the fourth-order diffusion coefficient is $D_{4g} = 0.081$ and 0.097, respectively. The values of D_{4g} were tested by varying the value by a factor of two to ensure that D_{4g} does not play a significant role in the dynamics.

[18] The inclusion of a guide field in these simulations changes the nature of reconnection relative to previous work on X-line spreading. In three-dimensional periodic domains, it is well established that the linear tearing instability is excited where $\mathbf{k} \cdot \mathbf{B}_0 = 0$, where $\mathbf{B}_0 = B_{x0}\hat{x} + B_{z0}\hat{z}$ is the equilibrium magnetic field and $\mathbf{k} = k_x\hat{x} + k_z\hat{z}$ is the wave vector of the mode. The periodic domain enforces that $k_x = 2\pi m/L_x$ and $k_z = 2\pi n/L_z$, where m and n are integer mode numbers which specify the number of X-lines in the x and z direction, respectively. In the absence of a guide field, this condition is only satisfied where $B_{x0} = 0$. With a guide field, it is satisfied wherever $q(y) = L_x B_z(y)/L_z B_x(y) = m/n$ is a rational number, where $q(y)$ is the safety factor well known in fusion applications. The y locations where $\mathbf{k} \cdot \mathbf{B}_0 = 0$ is satisfied are called rational surfaces, and for the equilibrium profile here, the modes are displaced from where $B_{x0} = 0$ by a distance $y_s = w_0 \tanh^{-1}(nL_xB_g/mL_zB_0)$. Thus, modes in our simulations are excited on multiple rational surfaces.

[19] Reconnection is seeded using a coherent magnetic perturbation localized in the out-of-plane direction of the form

$$B_{y1} = \sum_{k_x,k_z} \widetilde{B}_1 \sin(k_x x + k_z z) f_z(z), \tag{12}$$

where $\widetilde{B}_1 = 0.1$. Here, $f_z(z)$ is an envelope that localizes the perturbation in the out-of-plane direction and is given by $f_z(z) = \{\tanh[(z + w_{0z})/6] - \tanh[(z - w_{0z})/6]\}/2$. We use $w_{0z} = 1$; a plot of $f_z(z)$ is in Figure 2. Random magnetic perturbations that range from $m, n = 0$ to 20 with small amplitude $0.02 \ B_0$ are included with the initial conditions to break symmetry so that secondary islands are ejected.

[20] In early simulations, we initially excite only the $(m, n) = (1, 0)$ mode in equation (12). Even though this mode is the strongest perturbation, oblique modes with $n \neq 0$ grow from the noise and dominate the reconnection. This is consistent with recent particle-in-cell (PIC) simulations [*Daughton et al.*, 2011] and linear theory [*Baalrud et al.*, 2012]. Oblique modes in reconnection have been observed many times in fusion applications [see, e.g., *Grasso et al.*, 2007]. In light of these results, we include oblique modes in equation (12) and compare the results with the original simulations. The values of m and n are chosen so that the displacement y_s is less than w_0. In this study, $m = 1$ for all simulations and n ranges from 0 to 3. Initially exciting oblique modes has no noticeable effect on the results on the development of reconnection. Thus, the results of this study are expected to be independent of the modes used to seed reconnection. Note, although the modes are oblique, they are still quasi two-dimensional until they start interacting strongly. It was shown [*Schreier et al.*, 2011] that interacting oblique modes can prevent X-lines from spreading, so we focus on times early enough in the evolution that oblique mode interactions have not yet occurred.

4. Results

[21] To ensure numerical feasibility of the simulations in three dimensions, we benchmark the simulations in two
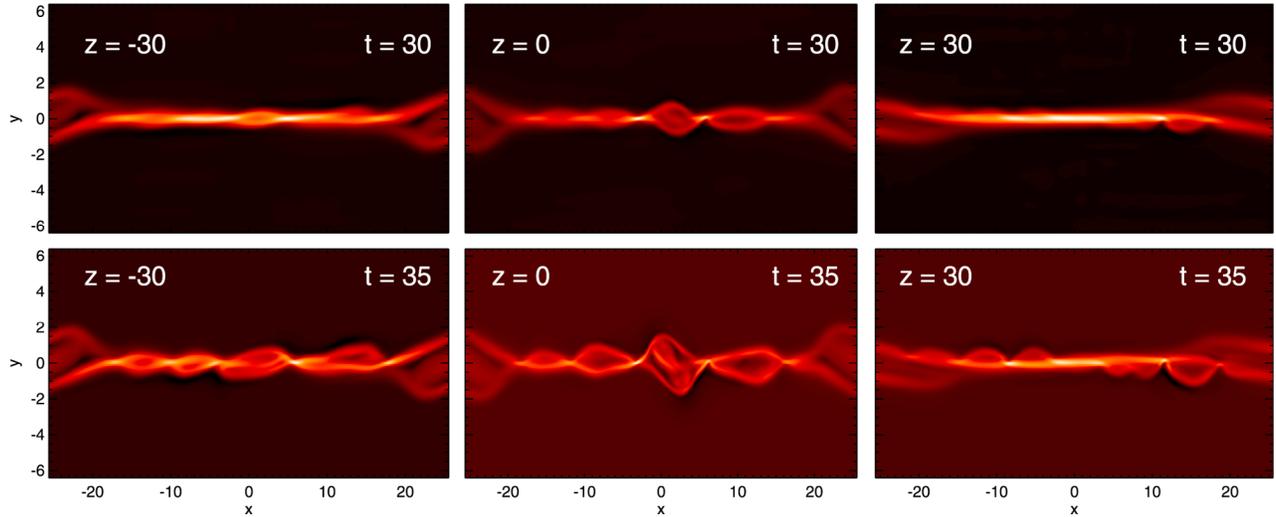
Figure 3. Cuts at different values of z of the out-of-plane current J_z for the $B_g = 3$ simulation. (top) At $t = 30$, Hall reconnection is developing at $z = 0$ but not at $z = \pm 30$. (bottom) At $t = 35$, Hall reconnection has developed fully at $z = 0$ and is developing at $z = \pm 30$.

dimensions. The simulations are evolved from $t = 0$ until nonlinear reconnection develops. In two dimensions, symmetry dictates that the $n = 0$ mode is the only excited mode. The reconnection rate E, measured as the time rate of change of the difference in magnetic flux between the X-line and O-line during a quasi-steady period, is approximately 0.08–0.1 [*Shay et al.*, 1999] for all simulations. Also, as expected, the time until Hall reconnection begins increases as the guide field increases since w_0 is held fixed, and there is a brief hyperresistive reconnection phase before onset for stronger guide fields.

[22] In the three-dimensional simulations, the evolution at $z = 0$ is very similar to what is observed in two dimensions: the timescale of the development of reconnection is comparable, and a hyperresistive phase precedes Hall reconnection. The reconnection rates can be compared, as well. The reconnection rate in three dimensions is measured by taking a cut of the z component of $\mathbf{v} \times \mathbf{B}$ in the y direction across the X-line; far from the current sheet, it asymptotes to the reconnection electric field in a steady state. The reconnection rates are in the 0.08–0.1 range, comparable to the two-dimensional results. One noticeable difference, as discussed earlier, is that oblique modes dominate over $n = 0$ modes in three dimensions.

[23] Each of the three-dimensional simulations display some form of X-line spreading. This can be seen qualitatively in Figure 3 for the simulation with $B_g = 3$. The out-of-plane current J_z at time $t = 30$ (Figure 3, top) and at time $t = 35$ (Figure 3, bottom) is displayed at three different out-of-plane positions: $z = -30$, 0, and 30 from left to right. At the earlier time $t = 30$, a transition to fast (Hall) reconnection at multiple sites at $z = 0$ has occurred, consistent with the development of multiple oblique modes. At $z = \pm 30$, the reconnection is still hyperresistive. At the later time $t = 35$, the current sheet at all three positions in z has developed multiple Hall reconnection X-lines. Thus, the Hall reconnection signal propagates bidirectionally from $z = 0$ for $B_g = 3$. It is worth noting that the multiple oblique mode reconnection seen here is consistent

with previous simulations, and the reason multiple X-lines appear despite the $m = 1$ mode being the dominant mode is that there are multiple modes simultaneously excited on different rational surfaces.

[24] To quantify the speed at which the X-line spreads, we must develop a systematic way to determine the extent of the reconnection region. As Hall reconnection develops, the out-of-plane current J_z at the X-line becomes noticeably higher than regions where reconnection is hyperresistive. For each slice in z, we measure the maximum out-of-plane current, which we call $J_{\max}(z)$. These maximum values of the current correspond to the location of the X-line for each position in z. The extent of the X-line can then be readily seen in a stack plot of $J_{\max}(z)$ as a function of t. Stack plots for all six initial guide fields in this study are displayed in Figure 4. As mentioned earlier, the plots only cover early times when the three-dimensional X-line structure is well defined because the interaction of oblique modes make defining the X-line structure prohibitive.

[25] The bright white regions in Figure 4 correspond to the strongest currents and, thus, the Hall reconnection X-lines. The dimmer areas outside of the white dashed lines (the red to black colors) indicate the region undergoing hyperresistive reconnection. As expected, the $B_g = 0$ simulation onsets almost immediately without a hyperresistive phase since $w_0 < d_i$, while the onset time increases as the guide field increases, leading to a longer hyperresistive phase. Both phases of reconnection spread in the z direction as time evolves; we focus on the Hall reconnection X-lines in the present study.

[26] From Figure 4, the qualitative differences in the nature of the spreading as a function of the guide field can readily be seen. For the strong guide field simulations $B_g \geq 2$, the X-line spreads symmetrically about $z = 0$ (Figure 4, top, which is consistent with our expectations for the strong guide field regime from equation (11). However, for simulations with a guide field weaker than the predicted condition $B_g < 2$, we observe different spreading behavior in the $+z$ and $-z$
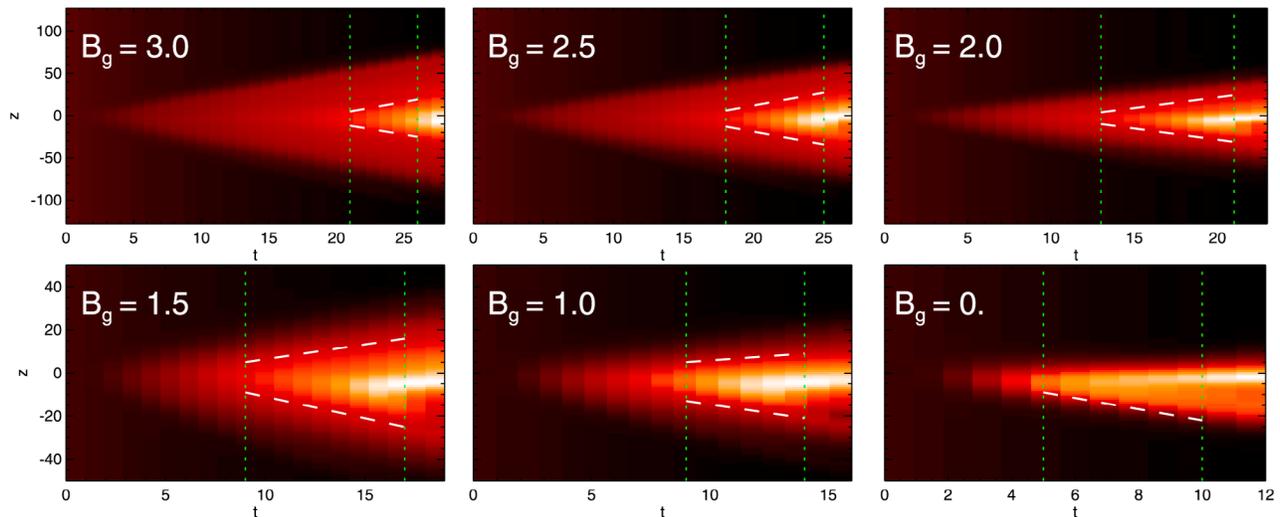
Figure 4. Stack plots of $J_{max}(z)$ as a function of t and z. The vertical dashed green lines indicate the range of time over which the spreading speed is measured, t_i and t_f. The dashed white lines indicate the extent in z of the X-line; their slope gives the speed of the spreading. Note the images in Figure 4 (bottom) are on a different scale in z than those in Figure 4 (top).

directions (Figure 4, bottom). For the $B_g = 1.5$ case, there is bidirectional spreading, as observed in the stronger guide field runs, but the spreading is not symmetric about $z = 0$. The spreading in the $-z$ direction appears marginally faster than in the $+z$ direction. These differences are further amplified in the $B_g = 1$ simulation. With no guide field ($B_g = 0$), spreading occurs primarily in the $-z$ direction, with negligible spreading in the $+z$ direction. Since J_z is in the $+z$ direction for this reconnection site, the propagation is in the direction of the electron out-of-plane flow, consistent with previous work [*Huba and Rudakov*, 2002].

[27] To make this quantitative, we measure the spreading speed of the X-line after Hall reconnection begins by finding the length of the X-line in the out-of-plane direction; its time rate of change between an initial and final time is the spreading speed. To do so, we note that the reconnection rate during hyperresistive reconnection never exceeds 0.01. We observe that when the out-of-plane Hall electric field $E_{Hg} = (\mathbf{J} \times \mathbf{B})_g/nec$ in a cut in the y direction through the X-line exceeds 0.01, the reconnection has begun its transition to Hall reconnection. We also note empirically that J_{max} at the time of this transition is always close to 3.3, which is robust for all the simulations performed here. Thus, we take Hall reconnection as occurring when J_{max} exceeds a threshold value of $J_{thresh} = 3.3$.

[28] The time frame over which the spreading speed is measured is defined as follows. The initial time t_i is defined as the earliest time that J_{max} exceeds J_{thresh} over the entire range from $z = \pm 5$. This range of z is chosen because the initial magnetic perturbation that seeds the reconnection is localized in this region, so genuine spreading not being influenced by the growth of reconnection inside the initially perturbed region requires the signal to leave this range in z. The final time t_f is defined for each simulation as the latest time in the evolution before multiple oblique modes interact; this assessment is done visually by finding where the current develops complicated structure as seen in Figure 3. The length

of the X-line at a given time is defined as the extent in z for which J_{max} exceeds J_{thresh}. The spreading speed is calculated as the difference of the length of the X-line between t_f and t_i divided by the time difference.

[29] An example of this procedure is presented in Figure 5, where representative data for the $B_g = 2.5$ simulation is shown. The initial time is $t_i = 18$, which is the earliest time that $J_{max} > J_{thresh}$ everywhere between $z = \pm 5$, as shown by the red dashed line. The final time is taken to be $t_f = 25$; a
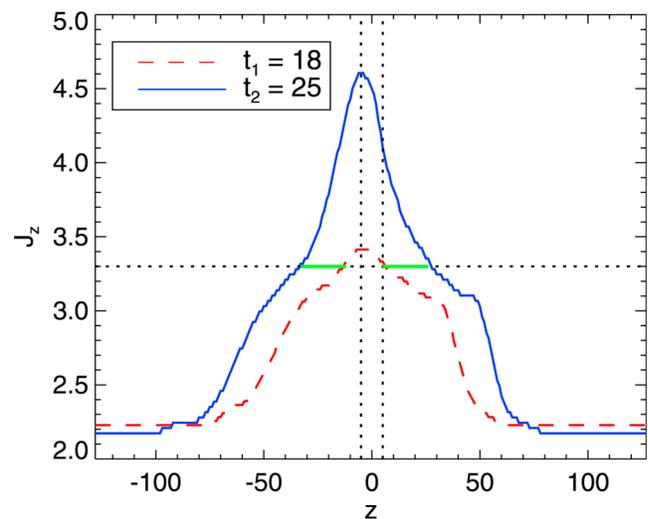
Figure 5. Cuts of the stack plot for the $B_g = 2.5$ case plotted in Figure 4. The dashed red line and solid blue line are at $t_i = 18$ and $t_f = 25$, respectively. The horizontal dotted line is at J_{thresh}, as defined in the text. The vertical dotted lines mark $z = \pm 5$, the approximate extent of the initial magnetic perturbation. The green line denotes the change in length of the X-line between t_i and t_f.
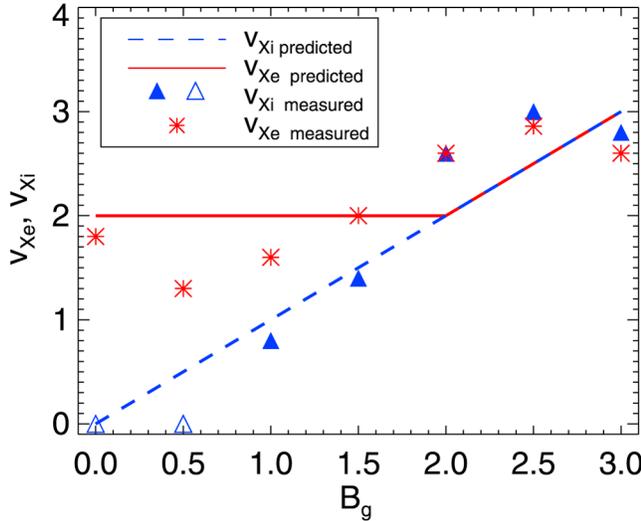
Figure 6. Spreading speeds v_{Xi} and v_{Xe} as a function of guide field B_g. The red asterisks are the measured values of v_{Xe}; the solid red line is the prediction from equation (3). The solid blue triangles are the measured values of v_{Xi}; the open triangles are for simulations for which no spreading was measured. The dashed blue line is the prediction from equation (6).

plot of $J_{\max}(z)$ at t_f is shown as the blue line. The horizontal dotted line marks the current threshold $J_{thresh} = 3.3$ and the vertical dotted lines mark the boundary of $z = \pm 5$. The change in length between the two times is the distance between the curves at J_{thresh}, marked by the green line segments. The lengths and speeds are calculated separately for the $\pm z$ direction because the speeds in the two directions may be different depending on the strength of the guide field. For the $B_g = 2.5$ simulation, the change in length in the $+z$ and $-z$ directions are 21 and 20 d_{i0}, respectively, and dividing by the time difference gives speeds of $v_{Xi} = 3.0\ c_{A0}$ for the speed in the $+z$ direction (the direction of ion out-of-plane flow) and $v_{Xe} = 2.9\ c_{A0}$ for the speed in the $-z$ direction (the direction of electron out-of-plane flow).

[30] The initial and final times t_i and t_f for each simulation are illustrated in Figure 4 as the vertical dotted green lines. The dashed white lines connect the extent of the X-line at the initial and final times. By inspection, one can see that the technique we employ to measure the extent of the X-line appropriately captures the evolution of the X-line length. Also, since the region of stronger current is rather straight between the beginning and final times, this implies the spreading speed is approximately constant in time.

[31] The measured X-line spreading speeds v_{Xe} and v_{Xi} are calculated as the time rate of change of the length of the X-line, which is equivalent to the slope of the white dashed lines in Figure 4. The results for the spreading speed in both directions are plotted as a function of guide field B_g in Figure 6. The measured value of the spreading speed is given by the solid blue triangles for v_{Xi} and the red stars for v_{Xe}. Note, v_{Xi} for $B_g = 0.0$ and 0.5 is plotted as zero as the hollow blue triangles. This is because the Hall reconnection signal is found to not extend past $z = \pm 5$ for either simulation during the time considered.

[32] To compare these results to the theory, note that the electrons carry all of the out-of-plane current in the $-z$ direction in our simulations. Therefore, in the weak guide field regime $B_g < 2$, equation (3) predicts that the spreading speed in the direction of the electron current v_{Xe} is the speed of the electrons given in equation (1), which is independent of B_g. When $B_g \geq 2$, the spreading speed is determined by the Alfvén speed given by equation (2), which increases linearly with B_g. The predicted speed of X-line spreading in the direction of the ion current v_{Xi} is the Alfvén speed due to the guide field, as given by equation (6), which increases linearly with B_g for all guide field strengths.

[33] The predicted spreading speeds v_{Xe} and v_{Xi} are depicted in Figure 6 by the solid red line and the dashed blue line, respectively. Qualitatively, the data reveal that the nature of X-line spreading is sensitive to the strength of the guide field. To interpret this more quantitatively, we first discuss the estimated uncertainties in our speed measurements. If we use a higher value of the current threshold J_{thresh}, the spreading speed changes on the order of 15–20%, which we take as the uncertainty. We note that for the large guide field runs $B_g \geq 2$, the speeds in either direction are within the uncertainties of each other. However, for $B_g < 2$, the speeds in either direction are separated by more than their uncertainty. These two results suggest that the spreading mechanism is the same in both directions for $B_g \geq 2$ and is different in either direction for $B_g < 2$, which quantitatively agrees with equation (11).

[34] For the absolute spreading speeds, when the estimated uncertainties are taken into account, the measured values agree with the predicted speeds. It is unexpected that the $B_g = 3$ speeds are slower than $B_g = 2.5$, but both are within the uncertainties of the predicted value. Also, it is expected that for $B_g = 0.5$, a nonzero value could be obtained if there had been a longer time before the oblique modes started interacting. Therefore, we conclude that data in Figure 6 quantitatively support the theory presented in section 2.

[35] In conclusion, the mechanism of X-line spreading in the out-of-plane direction is qualitatively different depending on the strength of the guide magnetic field. For $B_g \geq B_{crit,e}$, X-line spreading occurs bidirectionally along the guide field at the Alfvén speed. For $B_g \leq B_{crit,e}$, X-line spreading occurs bidirectionally along the guide field, but the spreading speed in the direction of the current carriers is the speed of the current carriers and in the direction opposite of the primary current carriers the spreading speed is the Alfvén speed. Measurements of X-line spreading for the hyperresistive reconnection that precedes Hall reconnection agree with the results obtained from measuring the Hall reconnection spreading (not shown). Therefore, the main result of this study applies both to Hall and hyperresistive reconnection in a two-fluid model.

5. Discussion

[36] In summary, the mechanism of X-line spreading in the out-of-plane direction is qualitatively different for strong guide magnetic fields than it is for weak guide fields. For weak guide fields, the reconnection signal is propagated by the current carriers, as has previously been established; for strong guide fields, the reconnection signal is propagated by Alfvén waves along the guide field. In general, the spreading speed in either out-of-plane direction is given by the

maximum of the speed of the current carriers in that direction and the Alfvén speed based on the guide field, as given by equation (9).

[37] Because the changeover from one spreading mechanism to the other is abrupt, there is a critical guide field strength (for each direction) at which the nature of the spreading switches. This critical field depends only on the strength of the reconnecting magnetic field, the ion inertial scale, the thickness of the electron dissipation region, and the fraction of the current carried by each species, as given by equation (10). When the guide field B_g exceeds the critical field, the spreading is due to Alfvén waves; when it is smaller, the spreading is due to the current carriers. The weak guide field result is consistent with previous numerical work of X-line spreading [*Huba and Rudakov*, 2002; *Shay et al.*, 2003; *Karimabadi et al.*, 2004; *Lapenta et al.*, 2006; *Nakamura et al.*, 2012], but the new result generalizes the predictions to include a guide field.

[38] The present results may be relevant for interpreting observations of reconnection in many settings. For example, in laboratory experiments, X-line spreading has been observed to be bidirectional and at the Alfvén speed in the strong guide field limit [*Katz et al.*, 2010] and unidirectional in the small guide field limit [*Dorfman*, 2012]. These results are consistent with the results of the present study.

[39] Another potential application is for solar flares. Two-ribbon flare evolution is marked by the ribbons moving apart from each other as time evolves, which is interpreted as newly reconnected field lines piling on top of previously reconnected field lines. In addition to this behavior, bidirectional spreading or elongation of the ribbon in the direction parallel to the ribbons along the polarity inversion line has been observed [*Qiu*, 2009]. It was shown that the spreading speed was consistent with the Alfvén speed [*Qiu*, 2009]. Since the reconnection driving the flare is most likely to have a sizable guide field, the present results suggest that this type of bidirectional spreading at the Alfvén speed would be expected.

[40] For an X2 flare on 7 November 2004, the spreading speed ranged between 10 and 70 km/s [*Qiu*, 2009]. Let us assume the spreading is governed by Alfvén waves. Assuming an average density of $n = 10^{13}$ cm^{-3} [*Qiu*, 2009], the guide field ranges from $B_g \simeq$ 15–100 G using equation (2). The motion of the ribbons normal to the ribbons was 20 km/s [*Qiu*, 2009], which is expected to be correlated to the inflow speed at the reconnection site. Since the inflow speed is often taken to be 0.1 of the Alfvén speed based on the reconnecting field, the reconnecting field strength $B_{rec} \simeq 140$ G. These results suggest the guide field is about 0.1–0.7 of the reconnecting field. The present results may be useful for inferring the guide field in flare observations. For comparison, from geometrical considerations of the magnetic fields of the flare loops, it was argued that the guide field in the Bastille Day flare was $B_g \simeq$ 0.4–1.2 times the reconnecting field [*Qiu et al.*, 2010]. Despite the large uncertainties, the two techniques give similar results. This analysis is obviously oversimplified and merely presented as an example of how the results can be used, but it is hoped that future work will allow for a meaningful assessment of the relative strengths of the guide and reconnecting fields. The reason this may be useful, as emphasized by *Qiu et al.* [2010], is that the strength of the guide field is known to

influence the production of secondary islands [*Drake et al.*, 2006b], and it has been suggested that the presence of secondary islands (plasmoids) is important for particle acceleration [*Drake et al.*, 2006a].

[41] Another interesting application is for reconnection in the solar wind, where reconnection X-lines extending hundreds of Earth radii have been reported [*Phan et al.*, 2006]. One can ask whether the spreading of reconnection in the out-of-plane direction could allow the X-line to be that long. To estimate the size of X-lines, assume that reconnection begins close to the Sun with an initially small finite length in the out-of-plane direction. Suppose the reconnection site convects out with the solar wind at a speed v_{SW}. (For simplicity, this calculation ignores variations in solar wind speed, magnetic field strength, and plasma density as a function of distance from the Sun.) Then, the time it takes to get to a position r_f away from the Sun is $t \sim r_f/v_{SW}$. If the speed of the spreading of the X-line is v_X, then the extent L of the X-line at r_f is $L \sim v_X t \sim r_f v_X/v_{SW}$, which gives the upper limit on the length of the X-line that could arise in the solar wind.

[42] One can test the implications of this from the observations of the reconnection event in the *Phan et al.* [2006] study, where a solar wind speed is inferred to be $v_{SW} = 340$ km/s. The satellite observations occurred near the Earth, so $r_f \simeq$ 1 AU $\simeq 2.3 \times 10^4 R_E$. The Alfvén speed based on a guide field of strength $B_g = 4$ nT and density $n = 20$ cm^3 [*Phan et al.*, 2006] is $c_{Ag} = 19$ km/s. If we take this as the spreading speed v_X, then the maximum length of the X-line is $L \sim r_f v_X/v_{SW} \sim 1.3 \times 10^3 R_E$. This exceeds the length of the X-line reported by *Phan et al.* [2006], which was 390 R_E. In this event, the strength of the guide field was 0.35 of the reconnecting field, so the Alfvén speed is the slower of the two velocities and the extent of the X-line if spreading is due to current carriers is even longer. Thus, while this calculation assumes that the reconnection proceeds at short distance from the Sun, it gives an indication that it is not impossible to achieve reconnection X-lines of the lengths reported by *Phan et al.* [2006]. Further work is necessary to make more careful comparisons of the theory to data.

[43] We conclude by collecting some assumptions of this work. We treat our system as quasi-two-dimensional, meaning any variation in the system in the direction of the current is negligible. The current sheets in all simulations performed are initially thin, meaning that free magnetic energy has already been stored. The plasma parameters across the current sheet are assumed symmetric. The simulations employ a two-fluid model, which does not fully capture electron scale physics. This may make quantitative changes to our results (such as the estimate of δ and the size of B_{rec}), but we do not expect qualitative changes to the theoretical results. Also, the simulations are isothermal and contain no thermal conduction.

[44] Another main assumption is that only a single mode is dominating the dynamics. However, the role of multiple oblique modes can play an important part of the dynamics of the spreading process. As seen in our simulations, the X-line structure is identifiable at early times but as the complicated nature of the oblique modes develop, the X-line structure break up due to the interaction between the current sheet. The interaction of oblique modes can impede X-line spreading [*Schreier et al.*, 2011]. More work is necessary on this topic.

References

Baalrud, S. D., A. Bhattacharjee, and Y. M. Huang (2012), Reduced magnetohydrodynamic theory of oblique plasmoid instabilities, *Phys. Plasmas*, *19*, 022101.

Birn, J., et al. (2001), GEM magnetic reconnection challenge, *J. Geophys. Res.*, *106*, 3715.

Cassak, P. A., and M. A. Shay (2007), Scaling of asymmetric magnetic reconnection: General theory and collisional simulations, *Phys. Plasmas*, *14*, 102114.

Daughton, W., V. Roytershteyn, H. Karimabadi, L. Yin, B. Albright, B. Bergen, and K. Bowers (2011), Role of electron physics in the development of turbulent magnetic reconnection in collisionless plasmas, *Nature*, *7*, 539.

Dorfman, S. E. (2012), Experimental study of 3-D, impulsive reconnection events in a laboratory plasma, PhD thesis, Princeton Univ., Princeton, N. J.

Drake, J. F., M. Swisdak, H. Che, and M. A. Shay (2006a), Electron acceleration from contracting magnetic islands during reconnection, *Nature*, *443*, 553.

Drake, J. F., M. Swisdak, K. M. Schoeffler, B. N. Rogers, and S. Kobayashi (2006b), Formation of secondary islands during magnetic reconnection, *Geophys. Res. Lett.*, *33*, L13105, doi:10.1029/2006GL025957.

Dungey, J. W. (1953), Conditions for the occurrence of electrical discharges in astrophysical systems, *Philos. Mag.*, *44*, 725.

Egedal, J., N. Katz, J. Bonde, W. Fox, A. Le, M. Porkolab, and A. Vrublevskis (2011), Spontaneous onset of magnetic reconnection in toroidal plasma caused by breaking of 2D symmetry, *Phys. Plasmas*, *18*, 111203.

Fuselier, S. A., H. U. Frey, K. J. Trattner, S. B. Mende, and J. L. Burch (2002), Cusp aurora dependence on interplanetary magnetic field B_z, *J. Geophys. Res.*, *107*(7), 1111, doi:10.1029/2001JA900165.

Grasso, D., D. Borgogno, and F. Pegoraro (2007), Secondary instabilities in two- and three-dimensional magnetic reconnection in fusion relevant plasmas, *Phys. Plasmas*, *14*, 055703.

Huba, J. D., and L. I. Rudakov (2002), Three-dimensional Hall magnetic reconnection, *Phys. Plasmas*, *9*, 4435.

Huba, J. D., and L. I. Rudakov (2003), Hall magnetohydrodynamics of neutral layers, *Phys. Plasmas*, *10*(8), 3139.

Isobe, H., K. Shibata, and S. Machida (2002), "Dawn-dusk asymmetry" in solar coronal arcade formations, *Geophys. Res. Lett.*, *29*(21), 2014, doi:10.1029/2001GL013816.

Jemella, B. D., M. A. Shay, J. F. Drake, and B. N. Rogers (2003), Impact of frustrated singularities on magnetic island evolution, *Phys. Rev. Lett.*, *91*, 125002.

Karimabadi, H., D. Krauss-Varban, J. D. Huba, and H. X. Vu (2004), On magnetic reconnection regimes and associated three-dimensional asymmetries: Hybrid, Hall-less hybrid, and Hall-MHD simulations, *J. Geophys. Res.*, *109*, A09205, doi:10.1029/2004JA010478.

Katz, N., J. Egedal, W. Fox, A. Le, J. Bonde, and A. Vrublevskis (2010), Laboratory observation of localized onset of magnetic reconnection, *Phys. Rev. Lett.*, *104*, 255004.

Lapenta, G., D. Krauss-Varban, H. Karimabadi, J. D. Huba, L. I. Rudakov, and P. Ricci (2006), Kinetic simulations of X-line expansion in 3D reconnection, *Geophys. Res. Lett.*, *33*, L10102, doi:10.1029/2005GL025124.

Lukin, V. S., and M. G. Linton (2011), Three-dimensional magnetic reconnection through a moving magnetic null, *Nonlinear Processes Geophys.*, *18*, 871.

McPherron, R. L., C. T. Russell, and M. P. Aubry (1973), Phenomenological model for substorms, *J. Geophys. Res.*, *78*, 3131.

Nagai, T. (1982), Observed magnetic substorm signatures at synchronous altitude, *J. Geophys. Res.*, *87*, 4405.

Nakamura, T. K. M., R. Nakamura, A. Alexandrova, Y. Kubota, and T. Nagai (2012), Hall magnetohydrodynamic effects for three-dimensional magnetic reconnection with finite width along the direction of the current, *J. Geophys. Res.*, *117*, A03220, doi:10.1029/2011JA017006.

Parker, E. N. (1957), Sweet's mechanism for merging magnetic fields in conducting fluids, *J. Geophys. Res.*, *62*, 509.

Petschek, H. E. (1964), Magnetic field annihilation, in *AAS/NASA Symposium on the Physics of Solar Flares*, edited by W. N. Ness, p. 425, NASA, Washington, D. C.

Phan, T. D., et al. (2000), Extended magnetic reconnection at the Earth's magnetopause from detection of bi-directional jets, *Nature*, *404*, 848.

Phan, T. D., et al. (2006), A magnetic reconnection X-line extending more than 390 Earth radii in the solar wind, *Nature*, *439*, 175.

Qiu, J. (2009), Observational analysis of magnetic reconnection sequence, *Astrophys. J.*, *692*, 1110.

Qiu, J., W. Liu, N. Hill, and M. Kazachenko (2010), Reconnection and energetics in two-ribbon flares: A revisit of the Bastille-Day flare, *Astrophys. J.*, *725*, 319.

Rogers, B. N., R. E. Denton, J. F. Drake, and M. A. Shay (2001), Role of dispersive waves in collisionless magnetic reconnection, *Phys. Rev. Lett.*, *87*, 195004.

Schreier, R., M. Swisdak, J. F. Drake, and P. A. Cassak (2011), Three-dimensional simulations of the orientation and structure of reconnection X-lines, *Phys. Plasmas*, *17*, 110704.

Shay, M. A., J. F. Drake, B. N. Rogers, and R. E. Denton (1999), The scaling of collisionless, magnetic reconnection for large systems, *Geophys. Res. Lett.*, *26*, 2163.

Shay, M. A., J. F. Drake, M. Swisdak, W. Dorland, and B. N. Rogers (2003), Inherently three-dimensional magnetic reconnection: A mechanism for bursty bulk flows?, *Geophys. Res. Lett.*, *30*(6), 1345, doi:10.1029/2002GL016267.

Shay, M. A., J. F. Drake, M. Swisdak, and B. N. Rogers (2004), The scaling of embedded collisionless reconnection, *Phys. Plasmas*, *11*, 2199.

Sweet, P. A. (1958), The neutral point theory of solar flares, in *Electromagnetic Phenomena in Cosmical Physics*, edited by B. Lehnert, p. 123, Cambridge Univ. Press, New York.

Tripathi, D., H. Isobe, and H. E. Mason (2006), On the propagation of brightening after filament/prominence eruptions, as seen by SoHO-EIT, *Astron. Astrophys.*, *453*(3), 1111.

Vasyliunas, V. M. (1975), Theoretical models of magnetic field line merging: 1, *Rev. Geophys.*, *13*, 303.

Zakharov, L., B. Rogers, and S. Migliuolo (1993), The theory of the early nonlinear stage of $m = 1$ reconnection in tokamaks, *Phys. Fluids B*, *5*, 2498.